ACS OMEGA

Article

Cite This: ACS Omega 2018, 3, 4392−4399

Transforming a C_3-Symmetrical Liquid Crystal to a π-Gelator by Alkoxy Chain Variation

Anjamkudy Sandeep,[†] Vakayil K. Praveen,[†,‡] D. S. Shankar Rao,[§] S. Krishna Prasad,[§] and Ayyappanpillai Ajayaghosh*[,†,‡]

[†]Photosciences and Photonics Section, Chemical Sciences and Technology Division, CSIR-National Institute for Interdisciplinary Science and Technology (CSIR-NIIST), Thiruvananthapuram 695019, India

[‡]Academy of Scientific and Innovative Research (AcSIR), CSIR-NIIST Campus, Thiruvananthapuram 695019, India

[§]Centre for Nano and Soft Matter Sciences (CeNS), Jalahalli, Bengaluru 560013, India

Supporting Information

ABSTRACT: Rational understanding of the structural features involving different noncovalent interactions is necessary to design a liquid crystal (LC) or an organogelator. Herein, we report the effect of the number and positions of alkoxy chains on the self-assembly induced physical properties of a few π-conjugated molecules. For this purpose, we designed and synthesized three C_3-symmetrical molecules based on oligo(*p*-phenylenevinylene), **C_3OPV1−3**. The self-assembly properties of these molecules are studied in the solid and solution states. All of the three molecules follow the isodesmic self-assembly pathway. Upon cooling from isotropic melt, **C_3OPV1** having nine alkoxy chains ($-OC_{12}H_{25}$) formed a columnar phase with two-dimensional rectangular lattice and retained the LC phase even at room temperature. Interestingly, when one of the $-OC_{12}H_{25}$ groups from each of the end benzene rings is knocked out, the resultant molecule, **C_3OPV2** lost the LC property, however, transformed as a gelator in toluene and *n*-decane. Surprisingly, when the $-OC_{12}H_{25}$ group from the middle position is removed, the resultant molecule **C_3OPV3** failed to form either the LC or the gel phases.

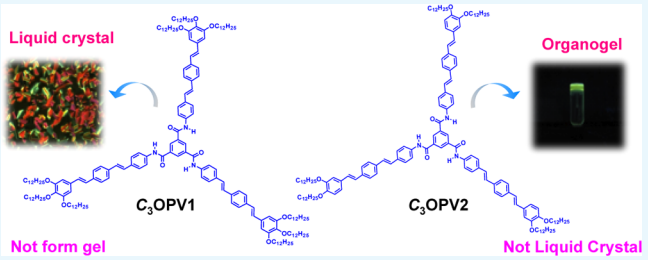

INTRODUCTION

Liquid crystals (LC) and gels are two distinct classes of soft materials of contemporary importance from the view point of basic and applied research.[1−12] Although a fundamental understanding of LCs has helped rational design and application of several subclasses,[1,2,4] the case of molecular gelators is mostly serendipitous.[3,10] However, the continued effort over the years has helped researchers to have a better understanding of the requirements of gelator design.[3−12] The knowledge acquired over the years in this direction has helped scientists to come up with several classes of molecular gelators. π-Gelators are one such class of functional soft materials.[5−7,9−12]

C_3-symmetrical platforms that are well exploited for the design of columnar LCs have also been reported to be suitable for the design of organogelators.[13−17] Therefore, we decided to explore the potential of C_3-symmetrical systems with one of the well-studied π-gelators, oligo(*p*-phenylenevinylenes) (OPV)[5,18−28] for the design of LC[29−31]-based π-gelators[32−37] to create multifunctional soft materials. In this process, we encountered an interesting observation of remarkable property variations of a C_3-symmetrical OPV molecule (**C_3OPV1**) when the terminal alkoxy chains are knocked out from different positions, to form the molecules **C3OPV2** and **C_3OPV3**. The chemical structures of **C_3OPV1−3** are shown in Figure 1.

RESULTS AND DISCUSSION

Synthesis of the C_3-symmetrical OPV molecules, **C_3OPV1−3** is shown in Schemes S1−S3. The *O*-alkylated benzaldehyde derivatives **2a−c** and the diethyl 4-(5,5-dimethyl-1,3-dioxan-2-yl)benzylphosphonate **7** were prepared as per reported procedures (Schemes S1 and S2).[38,39] The Wittig−Horner−Emmons olefination reaction of **2a−c** with the phosphonate **7** afforded compounds **8a−c** in 83−85% yield, which were then deprotected using trifluoroacetic acid to get the aldehydes **9a−c** in 87−92% yield. Afterward, the aldehydes **9a−c** were subjected to the Wittig−Horner−Emmons olefination reaction with diethyl(4-nitrobenzyl)phosphonate, resulting in the nitro derivatives **10a−c** in 80−85% yield. The nitro compounds **10a−c** were then reduced to the amino compounds **11a−c** using stannous chloride as the reducing agent in 80−85% yield. The OPV amine derivatives **11a−c** were then converted into the corresponding C_3-symmetrical OPVs by treating with trimesic acid trichloride (Scheme S3).[28,29] All of the reactions were carried out under dark condition to avoid the cis−trans isomerization of the olefinic double bond. The final molecules **C_3OPV1−3** were characterized using ^{1}H and ^{13}C NMR

Received: March 16, 2018
Accepted: April 13, 2018
Published: April 20, 2018

DOI: 10.1021/acsomega.8b00496
ACS Omega 2018, 3, 4392−4399

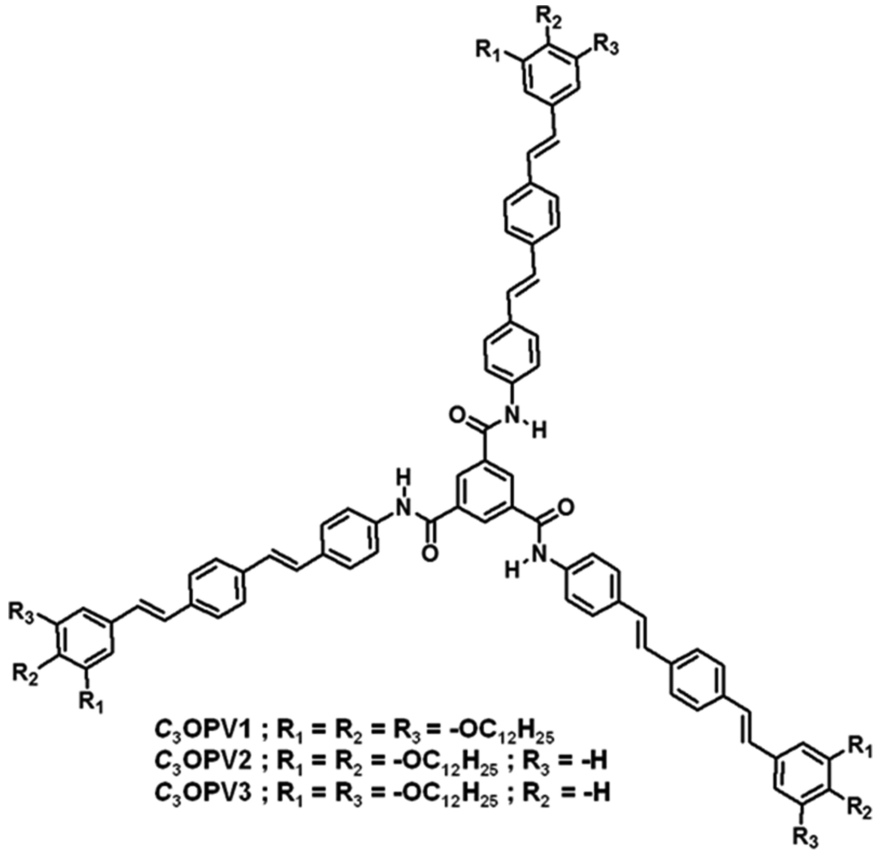

Figure 1. Molecular structures of C_3**OPV1−3**.

spectroscopy and matrix-assisted laser desorption ionization time-of-flight (MALDI-TOF) mass spectrometry (MS). Details of the synthetic procedures and the spectral characterization data of all intermediates are provided in the Supporting Information.

Having obtained the C_3-symmetrical OPV molecules in a pure form, our first objective was to study their physical properties. Optical polarizing microscopy (OPM) revealed that these compounds have high clearing temperature (the temperature at which the transition takes place from mesophase to the liquid state) and therefore get charred above 260 °C. Thus, to avoid such issues, the as-prepared sample was first heated to 260 °C and slowly cooled back to room temperature with a cooling rate of 5 K min^{-1}. In the case of **C_3OPV1**, upon cooling, a clear dendritic growth was observed with subsequent formation of strongly birefringent LC texture (Figure 2a). With further cooling, a mosaic pattern developed, which got retained right down to room temperature (Figure 2b). In a few cases, focal conics with stunted ends and stripes on the back of them were observed (Figure S1).

In view of the above features and with the support of the X-ray results to be described below, we identify the mesophase as a columnar phase with two-dimensional (2D) hexagonal/rectangular lattice at higher/lower temperatures. The observation of stripes in the low-temperature region further supports the rectangular nature of the lattice.[40,41] The other two derivatives **C_3OPV2** and **C_3OPV3** did not show any characteristic LC textures. Because of the decomposition of compounds at the clearing point, we were unable to characterize phase transitions using differential scanning calorimetry.

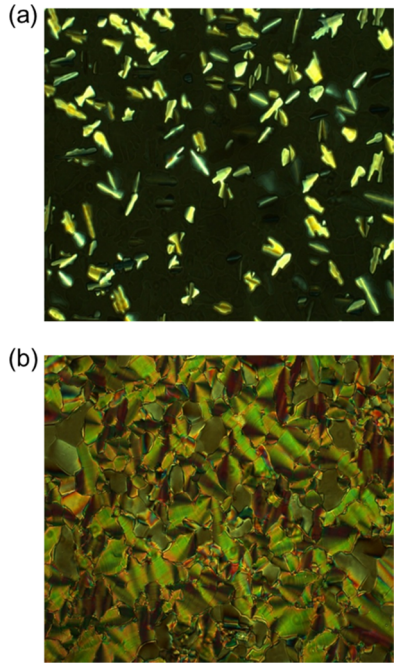

Figure 2. OPM images of **C_3OPV1** (a) at 250 °C and (b) at 28 °C upon cooling the sample from higher temperature (260 °C).

It has been reported that C_3-symmetrical design can generate large free volume if the compounds stack into columns and, consequently, destabilize the columnar stacks. However, the presence of 1,2,3-trialkoxybenzene groups can provide sufficient packing volume of the side chains to promote columnar

DOI: 10.1021/acsomega.8b00496
ACS Omega 2018, 3, 4392−4399

organization.[42−45] Thus, to gain more insight about columnar mesophase of **C_3OPV1**, detailed temperature-dependent X-ray diffraction (XRD) at different temperatures by cooling down the sample from 250 °C to room temperature (28 °C) has been carried out. The main panel of Figure 3 shows the XRD profiles

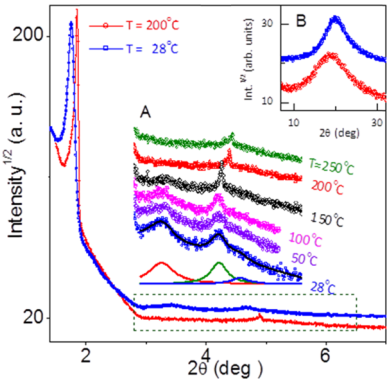

Figure 3. XRD profile of **C_3OPV1** at 200 °C (red) and 28 °C (blue). The low-angle region is shown in the main panel; the expansion (A) and the wide-angle portion (B) are shown in the inset.

of **C_3OPV1** in the low-angle region, obtained at 200 and 28 °C. At these temperatures, a very intense and sharp peak at low angles and a diffuse maximum at wide angles (inset B of Figure 3) were seen. In addition, a very weak but sharp peak was seen at intermediate angles. The intensity of this peak increases as the sample is cooled from 250 °C but interestingly, starts decreasing below 150 °C. Concomitantly, two diffuse maxima, one at the same angle as this peak and another at a slightly lower angle, developed (inset A of Figure 3).

The spacings corresponding to peaks at the lowest and intermediate angle are in the ratio of $1:1/\sqrt{7}$. Generally, for a hexagonal columnar packing, the ratio of the spacing of the small-angle peaks should be $1:1/\sqrt{3}:1/2:1/\sqrt{7}$, etc.[46−48] For **$C_3$OPV1**, considering the high-temperature region (T > 150 °C), the lattice can be indexed to be a hexagonal one, with the second ($1/\sqrt{3}$) and third (1/2) peaks absent. It may be recalled that there have been reports[36,49,50] wherein such a feature of certain peaks was found missing. In the present case, we can perhaps attribute it to the known tendency of the helical packing of the C_3-symmetrical amide units by a threefold H-bonding interaction.[17,49] At temperatures below 150 °C, the reflections could be indexed to a centered rectangular lattice, corroborating the OPM observations mentioned above. The results of the measured and calculated d-spacing, miller indices, and lattice parameters are summarized in Table S1. The effect of temperature on the spacing corresponding to the lowest angle peak is shown in Figure 4. The spacing increases somewhat abruptly around 150 °C, which can be associated with the transformation from a hexagonal to rectangular lattice.

A feature depicted in the inset A of Figure 3 that needs to be commented on is the weakening of the lattice reflections—specifically the reflections (21) at high temperature and (15) at low temperature—on cooling the sample below 150 °C. This observation is surprising because till room temperature, the mesophase remains the same. Even if there is a transition to a disordered phase, it is difficult to imagine that any pretransition effect would be spread over such a large temperature range. A possible explanation is that, at higher temperatures (T > 150 °C), the chains that would have significant gauche con-

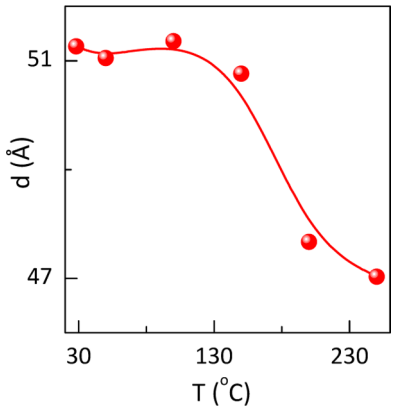

Figure 4. Thermal variation of the spacing of the low-angle peak.

formations owing to the substantial free space available may still permit a slightly better interaction between the cores of the neighboring molecules in the column. At lower temperatures, when the chains are quite stretched, adopting the all-trans conformation, a secondary effect may start dominating. The threefold H-bonding interaction (Figure S2) between the adjacent molecules in the column leads to a packing of the molecules in such a way that there is an angle of twist between them.[16,17,49,51] Such a requirement would weaken the lattice ordering, resulting in lower intensity for the reflections with higher Miller indices.

For a better understanding of the self-assembly, the absorption and emission spectra of all of the three molecules were monitored in different solvents and the results are tabulated in Table S2. The absorption spectra of **C_3OPV1** (1×10^{-4} M) in tetrahydrofuran (THF) and toluene showed almost similar spectral features, with a maximum around 380 nm (Figure S3a). For **C_3OPV2**, the absorption spectrum in THF (1×10^{-4} M) was found to be similar to that of **C_3OPV1**, with a maximum at 380 nm (Figure S3b). On the other hand, the absorption spectrum of **C_3OPV2** in toluene (1×10^{-4} M) showed blue-shifted (10 nm) absorption, with a maximum at 370 nm (Figure S3b). In the case of **C_3OPV3**, the absorption maximum in THF (1×10^{-4} M) was found at 370 nm (Figure S3c). The blue shift in the absorption maximum of **C_3OPV3** in THF when compared to that of the other two molecules could be due to the absence of an alkoxy group in the para position of the terminal benzene ring of the OPV unit. As in the case of **C_3OPV2**, the absorption maximum of **C_3OPV3** in toluene (1×10^{-4} M) also showed a blue shift of 10 nm (Figure S3c). In addition, both **C_3OPV2** and **C_3OPV3** displayed an additional shoulder band at longer wavelengths (425 nm), which disappeared at higher temperatures. From the absorption features of the molecules in THF and toluene, it is evident that both the **C_3OPV2** and **C_3OPV3** could form self-assembly in toluene, whereas it is less obvious in the case of **C_3OPV1**.

To gather insight about the mechanism of the self-assembly process,[52−59] temperature-dependent absorption studies were carried out. A 1×10^{-4} M solution of the compound in toluene was used for the studies. The absorption corresponding to the aggregation band at 425 nm was monitored as a function of temperature. The fraction of aggregates (α_{agg}) was then plotted against the temperature. Figure S4 shows a comparison of the melting transition curves obtained for **C_3OPV1** and **C_3OPV2** and a mixture of 10% (v/v) **C_3OPV2** in **C_3OPV1** (1×10^{-4} M). From this plot, it is clear that the melting transition

DOI: 10.1021/acsomega.8b00496
ACS Omega 2018, 3, 4392−4399

temperature, T_m (the temperature at which the α_{agg} is 50%) for **C_3OPV1** is 310.8 K and that for **C_3OPV2** is 321.5 K. The difference in the T_m values shows that **C_3OPV2** forms stronger assembly than **C_3OPV1**. To understand the effect of **C_3OPV2** on the self-assembly of **C_3OPV1**, we added 10 vol % 1×10^{-4} M **C_3OPV2** solution to **C_3OPV1** and the absorbance was monitored as a function of temperature. Interestingly, the melting transition temperature was found to increase from 310.8 to 314.8 K. This result implies that the presence of **C_3OPV2** increases the stability of the assembly formed by **C_3OPV1** due to the co-assembly of both molecules. The temperature-dependent absorption spectrum can be fitted with an isodesmic or equal-*K* model, in which each reversible step in the assembly pathway is characterized by a single association constant (K_e)[51−53,58,59] and the results are summarized in Figure S4 and Table 1. The gradual growth of the stacks with decreasing temperature, as shown in Figure S4, is a characteristic feature of isodesmic assembly. When compared with **C_3OPV1**, the degree of polymerization (DP_N) and K_e are found to be higher for **C_3OPV2**, indicating a better assembly. The increase found in the degree of polymerization (DP_N) of **C_3OPV1** from 2.1 to 2.4 in the presence of 10% (v/v) **C_3OPV2** suggests that **C_3OPV2** assists the assembly process of **C_3OPV1**.[60]

Table 1. Thermodynamic Parameters for the Self-Assembly of C_3OPV1, C_3OPV2, and a Mixture of 10% (v/v) C_3OPV2 in C_3OPV1 Obtained Using the Isodesmic Model[a,b]

molecule	ΔH (kJ mol^{-1})	ΔS (J mol^{-1} K^{-1})	T_m (K)	K_e (10^4 M^{-1})	DP_N
C_3OPV1	−103.75	−248.67	310.8	2.4	2.1
C_3OPV2	−85.10	−194.5	321.4	4.7	2.5
10% (v/v) **C_3OPV2** in **C_3OPV1**	−97.28	−237.44	314.8	3.5	2.4

[a]All studies were conducted in toluene (1×10^{-4} M). [b]ΔH is the change in enthalpy, ΔS is the change in entropy, T_m is the melting transition temperature, K_e is the association constant, and DP_N is the degree of polymerization.

Subsequently, we studied the fluorescence properties of **C_3OPV1−3** (1×10^{-4} M). For **C_3OPV1**, the emission maximum in toluene and THF remained the same at 435 nm but the emission intensity was found to be less in the case of toluene (Figure 5a). In THF, **C_3OPV2** showed an emission maximum at 431 nm and in toluene, the emission maximum displayed a red shift of 70 nm (λ_{max} = 504 nm) with a broadening of the spectrum (Figure 5b). The quenching of fluorescence with broadening implies the formation of supramolecular assembly of **C_3OPV2** in toluene. The **C_3OPV3** molecule displayed almost similar emission features in both toluene and THF with slightly enhanced emission in toluene (Figure 5c).

To know the nature of interaction between the molecules and with the solvents and also to understand the kind of assembly formed in these solvents, detailed morphological studies were carried out. In the case of nonpolar solvents, the molecule−solvent interactions are minimum and hence the molecule−molecule noncovalent forces may play a major role in the self-assembly of molecules.[8,61−64] With the help of atomic force microscopy (AFM), the morphological studies were carried out. In the case of **C_3OPV1**, due to weak assembly in toluene or other nonpolar solvents, the molecule−solvent interaction will be more, resulting in spherical particles at a concentration of 1×10^{-4} M (Figure 6a). At the same concentration, **C_3OPV2** in toluene formed intertwined fibers of micrometer length, with an average diameter of 250 nm (Figure 6b). The formation of these extended assemblies can be due to the long-range interaction of **C_3OPV2** molecules via H-bonding, π-stacking, and van der Waals interactions. On the other hand, **C_3OPV3** fails to form such extended assembly and instead, assembles together to form spherical particles (Figure

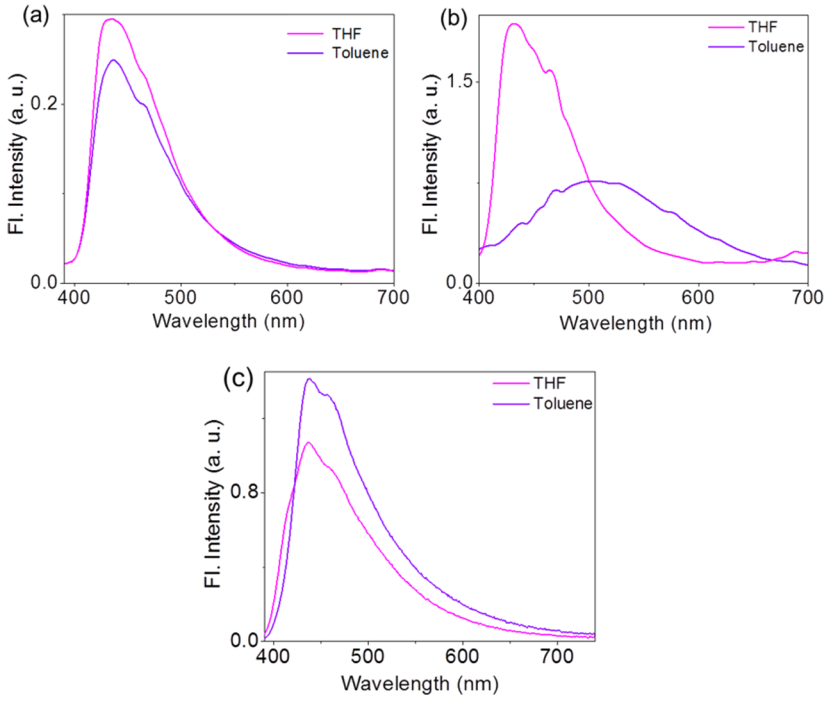

Figure 5. Emission spectra of (a) **C_3OPV1**, (b) **C_3OPV2**, and (c) **C_3OPV3** in THF and toluene (1×10^{-4} M); λ_{ex} = 375 nm.

DOI: 10.1021/acsomega.8b00496
ACS Omega 2018, 3, 4392−4399

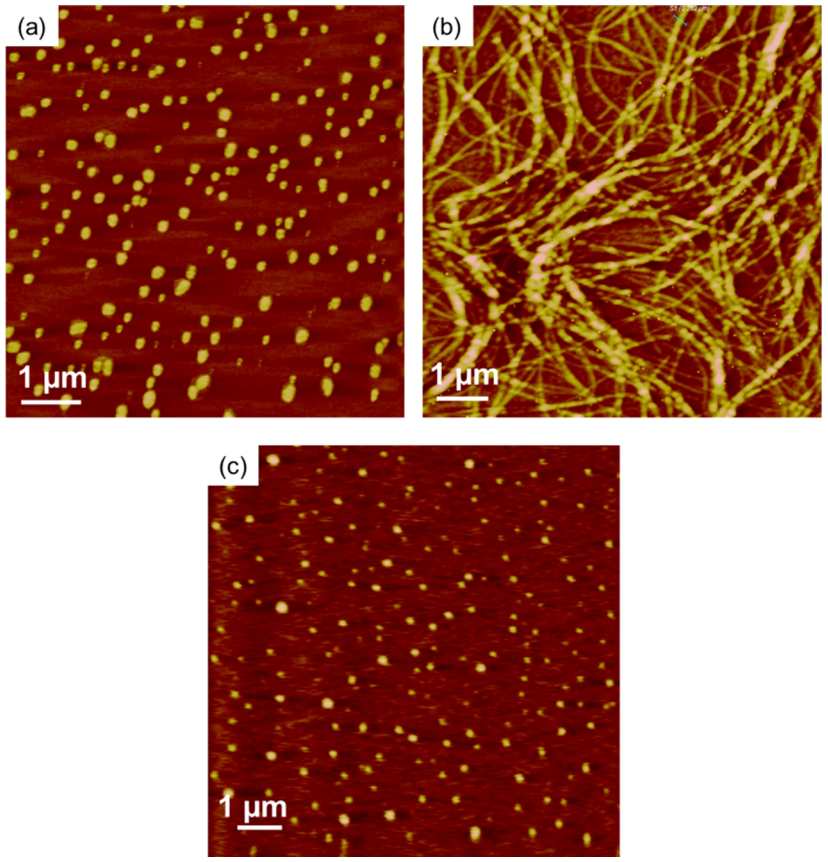

Figure 6. AFM images of (a) C_3**OPV1**, (b) C_3**OPV2**, and (c) C_3**OPV3** in toluene on mica surface. In all of the cases, the concentration of the solution used is 1×10^{-4} M.

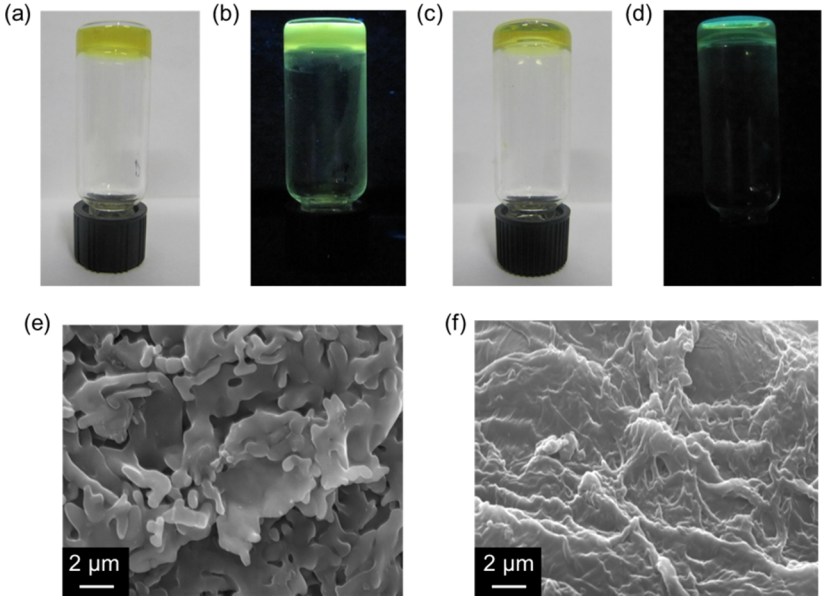

Figure 7. Photograph of C_3**OPV2** gel formed in (a) and (b) in *n*-decane and in (c) and (d) in toluene under normal light and under UV light (λ_{ex} = 365 nm), respectively. Scanning electron microscopy (SEM) images of C_3**OPV2** (e) *n*-decane and (f) toluene gel, respectively.

6c). The spherical particle size distribution of both C_3**OPV1** and C_3**OPV3** is given in Figure S5. In the case of C_3**OPV1**, the size of the particle varies from 150 to 300 nm, with maximum number of particles having an average size of 220 nm. Similarly, for C_3**OPV3**, the size distribution is almost similar to that of C_3**OPV1**, with an average size of around 210 nm.

The gelation properties of these molecules were then studied and it was found that only C_3**OPV2** was able to form gel (Table S3). The other two molecules failed to form gel in any of the solvents tested. C_3**OPV2** was able to form gel in toluene, *n*-decane, cyclohexane, methylcyclohexane, etc. As in the case of other C_3-symmetrical molecules, C_3**OPV2** needs very high

DOI: 10.1021/acsomega.8b00496
ACS Omega 2018, 3, 4392−4399

concentration to form the gel.[13,65] The minimal gelator concentration (MGC) for **C_3OPV2** in toluene is 4.65 mM. In cyclohexane and methylcyclohexane, the MGC is found to be 14.86 and 13.94 mM, respectively, which is almost 3 times higher than that required for the gelation in toluene. Furthermore, a solvent-dependent difference in the nature of the gel was noticed. In toluene, a transparent gel was formed, whereas other solvents gels were found to be opaque (Figure 7a–d). The lack of gelation property of **C_3OPV1** and **C_3OPV3** can be rationalized on the basis of their morphology. Gelation is basically the entrapment of solvents inside a three-dimensional solid matrix of interconnected network of fibers.[3,10,63] Scanning electron microscopy (SEM) studies revealed that **C_3OPV2** forms extended structures in the gel phase (Figure 7e,f). In *n*-decane, extended sheetlike features are seen, whereas in toluene, large fiber bundles are formed. However, the other two molecules, i.e., **C_3OPV1** and **C_3OPV3**, were unable to form such sheets or fibrous assembly. Therefore, **C_3OPV1** and **C_3OPV3** could not entrap solvent molecules and therefore gelation was not observed.

The weak assembly of **C_3OPV1** in toluene can be attributed to the presence of nine alkoxy chains around the central C_3 core, which facilitate high solubility for the molecule in this solvent. At the same time, when one of the alkoxy chains from each arm of the **C_3OPV1** is removed, as in the case of **C_3OPV2** or as in the case of **C_3OPV3**, the solubility in toluene and other nonpolar solvents get reduced, forcing the molecule to form assembly with the help of H-bonding, $\pi-\pi$ stacking, and van der Waals interactions.

CONCLUSIONS

In conclusion, the present study is an example of structural engineering by which an LC mesophase forming C_3-symmetrical molecule can be transformed into an organogelator. **C_3OPV1**, the molecule with nine alkoxy chains at the periphery of the disc, shows mesomorphic properties even at room temperature and the LC phase is identified as columnar phase with 2D rectangular lattice. As the number of alkoxy chains at the periphery decreases, the LC property disappears. **C_3OPV2**, a molecule with alkoxy chains at 3,4-positions is able to gelate organic solvents, whereas **C_3OPV3**, a molecule with alkoxy chains at 3,5-positions, neither forms gel nor shows any LC properties. This study illustrates the important role of alkoxy chains in the design of functional molecules with distinctly different properties[48,66−68] and hence can be applied to several of the existing systems for their rational conversion to functional soft materials.

EXPERIMENTAL SECTION

General Procedure for the Synthesis of C_3OPV1−3. These molecules were synthesized according to Scheme S3. To a solution of OPV amine **11a−c** (0.15 mmol) and triethylamine (0.5 mL) in dry dichloromethane (10 mL), a solution of trimesic acid trichloride (0.045 mmol) was added dropwise. The mixture was stirred for 6 h, and the solvent was evaporated under reduced pressure. Purification by column chromatography on silica gel (dichloromethane−*n*-hexane 3:1) and Bio-Beads SX-1 (dichloromethane) yielded pure **C_3OPV1−3**.

C_3OPV1. Yield: 45%; ^{1}H NMR (300 MHz, THF-d_8): δ = 11.14 (s, 3H), 10.21 (s, 3H), 8.78 (s, 3H), 7.91−7.53 (m, 18H), 7.19−7.04 (m, 18H), 6.82 (s, 3H), 4.02−3.82 (m, 18H), 1.77−1.31 (m, 180H) 0.89 (s, 27H) ppm; ^{13}C NMR (125 MHz, $CDCl_3$): δ = 13.8, 23.7, 25.4, 29.9, 30.2, 32.4, 69.6, 118.3, 124.7, 126.8, 127.4, 129.2, 129.3, 133.2, 134.7, 137.2, 147.5, 165.2 ppm; MALDI-TOF-MS: m/z calculated for $C_{183}H_{273}N_3O_{12}$ $[M^+]$ is 2707.14; found: 2707.63.

C_3OPV2. Yield: 50%; ^{1}H NMR (300 MHz, THF-d_8): δ = 11.00 (s, 3H), 9.94 (s, 3H), 8.78 (s, 3H), 7.9−7.87 (d, 6H), 7.77−7.41 (m, 16H), 7.19−7.03 (m, 14H), 6.78 (s, 6H), 4.02−3.82 (m 12H), 1.77−1.31 (m, 180H) 0.89 (s, 18H) ppm; ^{13}C NMR (125 MHz, $CDCl_3$): δ = 11.6, 20.7, 22.2, 29.6, 29.8, 31.8, 65.2, 73.8, 102.8, 118.3, 124.6, 124.8, 125.4, 134, 136.7, 138.1, 153.5, 165.2 ppm; MALDI-TOF-MS: m/z calculated for $C_{147}H_{201}N_3O_9$ $[M^+]$ is 2155.20; found 2155.23.

C_3OPV3. Yield: 42%; ^{1}H NMR (300 MHz, THF-d_8): δ = 11.12 (s, 3H), 10.07 (s, 3H), 8.67 (s, 3H), 7.79−7.77 (d, 6H), 7.44−7.41 (m, 16H), 7.06−6.91 (m, 14H), 6.78 (s, 6H), 4.02−3.82 (m 12H), 1.77−1.31 (m, 180H) 0.89 (s, 18H) ppm; ^{13}C NMR (125 MHz, $CDCl_3$): δ = 11.4, 21.3, 22.2, 29.7, 29.8, 31.2, 65.0, 72.6, 102.6, 116.1, 124.0, 124.6, 125.2, 134.2, 136.8, 138.7, 153.1, 165.2 ppm; MALDI-TOF-MS: m/z calculated for $C_{147}H_{201}N_3O_9$ $[M^+]$ is 2155.20; found: 2155.74.

Optical Polarizing Microscopy. Liquid crystalline phase transitions and optical anisotropy were observed using a Leica DFC 490 polarized light optical microscope, equipped with a Mettler TOLEDO FP82HT (temperature programmer) heating and freezing stage.

X-ray Diffraction. Temperature-dependent X-ray diffraction studies of the liquid crystalline phases were carried out on samples filled in Lindemann capillaries and were held at required temperatures using a Mettler hot stage and irradiated with Cu Kα radiation (λ = 1.5418 Å). The apparatus essentially involved a high-resolution X-ray powder diffractometer (PANalytical X'Pert PRO) equipped with a high-resolution fast detector, PIXCEL.

Optical Measurements. The electronic absorption spectra were recorded on a Shimadzu UV-2600 UV−vis scanning spectrophotometer equipped with peltier thermostatic cell holders. The fluorescence spectra were recorded on a SPEX-Fluorolog F112X spectrofluorimeter.

Atomic Force Microscopy. AFM images were recorded under ambient conditions using NTEGRA (NT-MDT) operated with a tapping mode regime. Microfabricated TiN cantilever tips (NSG10) with a resonance frequency of 299 kHz and a spring constant of S8 20−80 N m^{-1} were used. Samples for the imaging were prepared by drop casting solution of **C_3OPV1−3** in toluene (1×10^{-4} M) on freshly cleaved mica surface. The samples were first air-dried and further dried under vacuum.

Scanning Electron Microscopy. SEM images were taken on a Zeiss EVO 18 cryo SEM Special Edn with a variable pressure detector working at 20−30 kV after sputtering with gold. Samples were prepared by drop casting the gel on a freshly cleaved mica substrate. They were kept overnight to allow slow evaporation of the solvent and further dried in a vacuum desiccator for 12 h.

ASSOCIATED CONTENT

Supporting Information

The Supporting Information is available free of charge on the ACS Publications website at DOI: 10.1021/acsomega.8b00496.

Materials and methods, synthesis schemes, procedures and characterization data of all intermediate compounds, additional tables and figures (PDF)

DOI: 10.1021/acsomega.8b00496
ACS Omega 2018, 3, 4392−4399

AUTHOR INFORMATION

Corresponding Author

*E-mail: ajayaghosh@niist.res.in.

ORCID

Vakayil K. Praveen: 0000-0002-5407-9901
D. S. Shankar Rao: 0000-0002-9643-6604
S. Krishna Prasad: 0000-0002-9367-1369
Ayyappanpillai Ajayaghosh: 0000-0001-8574-5391

Author Contributions

The manuscript was written through contributions of all authors.

Notes

The authors declare no competing financial interest.

ACKNOWLEDGMENTS

A.A. is grateful to the Department of Science and Technology (DST-SERB), Government of India, for the J.C. Bose Fellowship (SB/S2/JCB-11/2014). A.S. is grateful for a research fellowship from the CSIR, Government of India. V.K.P. acknowledges DST, Government of India for the Young Scientist Fellowship (SB/FT/CS-131/2014).

REFERENCES

(1) Chandrasekhar, S. *Liquid Crystals*, 2nd ed.; University Press: Cambridge, 1992.

(2) Goodby, J. W., Collings, P. J., Kato, T., Tschierske, C., Gleeson, H., Raynes, P., Eds.; *Handbook of Liquid Crystals*, 2nd ed.; Wiley-VCH: Weinheim, 2014.

(3) Terech, P.; Weiss, R. G. Low Molecular Mass Gelators of Organic Liquids and the Properties of Their Gels. *Chem. Rev.* **1997**, *97*, 3133−3160.

(4) Kato, T.; Hirai, Y.; Nakaso, S.; Moriyama, M. Liquid-Crystalline Physical Gels. *Chem. Soc. Rev.* **2007**, *36*, 1857−1867.

(5) Ajayaghosh, A.; Praveen, V. K. π-Organogels of Self-Assembled *p*-Phenylenevinylenes: Soft Materials with Distinct Size, Shape, and Functions. *Acc. Chem. Res.* **2007**, *40*, 644−656.

(6) Maeda, H. Anion-Responsive Supramolecular Gels. *Chem. − Eur. J.* **2008**, *14*, 11274−11282.

(7) Ajayaghosh, A.; Praveen, V. K.; Vijayakumar, C. Organogels as Scaffolds for Excitation Energy Transfer and Light Harvesting. *Chem. Soc. Rev.* **2008**, *37*, 109−122.

(8) Li, J.-L.; Liu, X.-Y. Architecture of Supramolecular Soft Functional Materials: From Understanding to Micro-/Nanoscale Engineering. *Adv. Funct. Mater.* **2010**, *20*, 3196−3216.

(9) Dawn, A.; Shiraki, T.; Haraguchi, S.; Tamaru, S.-i.; Shinkai, S. What Kind of "Soft Materials" Can We Design From Molecular Gels? *Chem. − Asian J.* **2011**, *6*, 266−282.

(10) Babu, S. S.; Praveen, V. K.; Ajayaghosh, A. Functional π-Gelators and Their Applications. *Chem. Rev.* **2014**, *114*, 1973−2129.

(11) Praveen, V. K.; Ranjith, C.; Armaroli, N. White-Light-Emitting Supramolecular Gels. *Angew. Chem., Int. Ed.* **2014**, *53*, 365−368.

(12) Ghosh, S.; Praveen, V. K.; Ajayaghosh, A. The Chemistry and Applications of π-Gels. *Annu. Rev. Mater. Res.* **2016**, *46*, 235−262.

(13) van Gorp, J. J.; Vekemans, J. A. J. M.; Meijer, E. W. C_3-Symmetrical Supramolecular Architectures: Fibers and Organic Gels from Discotic Trisamides and Trisureas. *J. Am. Chem. Soc.* **2002**, *124*, 14759−14769.

(14) Aparicio, F.; García, F.; Sánchez, L. Supramolecular Polymerization of C_3-Symmetric Organogelators: Cooperativity, Solvent, and Gelation Relationship. *Chem. − Eur. J.* **2013**, *19*, 3239−3248.

(15) Pop, F.; Melan, C.; Danila, I.; Linares, M.; Beljonne, D.; Amabilino, D. B.; Avarvari, N. Hierarchical Self-Assembly of Supramolecular Helical Fibres from Amphiphilic C_3-Symmetrical Functional Tris(tetrathiafulvalenes). *Chem. − Eur. J.* **2014**, *20*, 17443−17453.

(16) Cantekin, S.; de Greef, T. F. A.; Palmans, A. R. A. Benzene-1,3,5-Tricarboxamide: A Versatile Ordering Moiety for Supramolecular Chemistry. *Chem. Soc. Rev.* **2012**, *41*, 6125−6137.

(17) Kulkarni, C.; Meijer, E. W.; Palmans, A. R. A. Cooperativity Scale: a Structure−Mechanism Correlation in the Self-Assembly of Benzene-1,3,5-Tricarboxamides. *Acc. Chem. Res.* **2017**, *50*, 1928−1936.

(18) Ajayaghosh, A.; Praveen, V. K.; Srinivasan, S.; Varghese, R. Quadrupolar π-Gels: Sol−Gel Tunable Red−Green−Blue Emission in Donor−Acceptor-Type Oligo(*p*-phenylenevinylene)s. *Adv. Mater.* **2007**, *19*, 411−415.

(19) Babu, S. S.; Praveen, V. K.; Prasanthkumar, S.; Ajayaghosh, A. Self-Assembly of Oligo(*para*-phenylenevinylene)s through Arene-Perfluoroarene Interactions: π Gels with Longitudinally Controlled Fiber Growth and Supramolecular Exciplex-Mediated Enhanced Emission. *Chem. − Eur. J.* **2008**, *14*, 9577−9584.

(20) Yagai, S.; Kubota, S.; Unoike, K.; Karatsu, T.; Kitamura, A. Cyanurate-Guided Self-Assembly of a Melamine-Capped Oligo(*p*-phenylenevinylene). *Chem. Commun.* **2008**, 4466−4468.

(21) Kumar, V. R. R.; Sajini, V.; Sreeprasad, T. S.; Praveen, V. K.; Ajayaghosh, A.; Pradeep, T. Probing the Initial Stages of Molecular Organization of Oligo(*p*-phenylenevinylene) Assemblies with Monolayer Protected Gold Nanoparticles. *Chem. − Asian J.* **2009**, *4*, 840−848.

(22) Samanta, S. K.; Pal, A.; Bhattacharya, S. Choice of the End Functional Groups in Tri(*p*-phenylenevinylene) Derivatives Controls Its Physical Gelation Abilities. *Langmuir* **2009**, *25*, 8567−8578.

(23) Babu, S. S.; Praveen, V. K.; Kartha, K. K.; Mahesh, S.; Ajayaghosh, A. Effect of the Bulkiness of the End Functional Amide Groups on the Optical, Gelation, and Morphological Properties of Oligo(*p*-phenylenevinylene) π-Gelators. *Chem. − Asian J.* **2014**, *9*, 1830−1840.

(24) Yao, C.; Lu, Q.; Wang, X.; Wang, F. Reversible Sol-Gel Transition of Oligo(*p*-phenylenevinylene)s by π-π Stacking and Dissociation. *J. Phys. Chem. B* **2014**, *118*, 4661−4668.

(25) Praveen, V. K.; Ranjith, C.; Bandini, E.; Ajayaghosh, A.; Armaroli, N. Oligo(phenylenevinylene) Hybrids and Self-Assemblies: Versatile Materials for Excitation Energy Transfer. *Chem. Soc. Rev.* **2014**, *43*, 4222−4242.

(26) Kartha, K. K.; Praveen, V. K.; Babu, S. S.; Cherumukkil, S.; Ajayaghosh, A. Pyridyl-Amides as a Multimode Self-Assembly Driver for the Design of a Stimuli Responsive π-Gelator. *Chem. − Asian J.* **2015**, *10*, 2250−2256.

(27) Ardoña, H. A. M.; Kale, T. S.; Ertel, A.; Tovar, J. D. Nonresonant and Local Field Effects in Peptidic Nanostructures Bearing Oligo(*p*-phenylenevinylene) Units. *Langmuir* **2017**, *33*, 7435−7445.

(28) Sandeep, A.; Praveen, V. K.; Kartha, K. K.; Karunakaran, V.; Ajayaghosh, A. Supercoiled Fibres of Self-Sorted Donor-Acceptor Stacks: A Turn-Off/Turn-on Platform for Sensing Volatile Aromatic Compounds. *Chem. Sci.* **2016**, *7*, 4460−4467.

(29) van Herrikhuyzen, J.; Jonkheijm, P.; Schenning, A. P. H. J.; Meijer, E. W. The Influence of Hydrogen Bonding and π−π Stacking Interactions on the Self-Assembly Properties of C_3-Symmetrical Oligo(*p*-phenylenevinylene) Discs. *Org. Biomol. Chem.* **2006**, *4*, 1539−1545.

(30) Lehmann, M.; Hügel, M. A Perfect Match: Fullerene Guests in Star-Shaped Oligophenylenevinylene Mesogens. *Angew. Chem., Int. Ed.* **2015**, *54*, 4110−4114.

(31) Lehmann, M.; Maier, P. Shape-Persistent, Sterically Crowded Star Mesogens: From Exceptional Columnar Dimer Stacks to Supermesogens. *Angew. Chem., Int. Ed.* **2015**, *54*, 9710−9714.

(32) Yagai, S.; Kinoshita, T.; Higashi, M.; Kishikawa, K.; Nakanishi, T.; Karatsu, T.; Kitamura, A. Diversification of Self-Organized Architectures in Supramolecular Dye Assemblies. *J. Am. Chem. Soc.* **2007**, *129*, 13277−13287.

(33) Kato, T.; Tanabe, K. Electro-and Photoactive Molecular Assemblies of Liquid Crystals and Physical Gels. *Chem. Lett.* **2009**, *38*, 634−639.

DOI: 10.1021/acsomega.8b00496
ACS Omega 2018, 3, 4392−4399

(34) Saito, N.; Kanie, K.; Matsubara, M.; Muramatsu, A.; Yamaguchi, M. Dynamic and Reversible Polymorphism of Self-Assembled Lyotropic Liquid Crystalline Systems Derived From Cyclic Bis-(ethynylhelicene) Oligomers. *J. Am. Chem. Soc.* **2015**, *137*, 6594−6601.
(35) Görl, D.; Soberats, B.; Herbst, S.; Stepanenko, V.; Würthner, F. Perylene Bisimide Hydrogels and Lyotropic Liquid Crystals with Temperature-Responsive Color Change. *Chem. Sci.* **2016**, *7*, 6786−6790.
(36) Pradhan, B.; Vaisakh, V. M.; Nair, G. G.; Rao, D. S. S.; Prasad, S. K.; Sudhakar, A. A. Effect of Atomic-Scale Differences on the Self-Assembly of Thiophene-Based Polycatenars in Liquid Crystalline and Organogel States. *Chem. − Eur. J.* **2016**, *22*, 17843−17856.
(37) Sivadas, A. P.; Rao, D. S. S.; Kumar, N. S. S.; Prabhu, D. D.; Varghese, S.; Ramachandran, C. N.; Ongungal, R. M.; Krishna Prasad, S.; Das, S. Self-Assembling and Luminescent Properties of Chiral Bisoxadiazole Derivatives in Solution and Liquid-Crystalline Phases. *J. Phys. Chem. B* **2017**, *121*, 1922−1929.
(38) Eckert, J.-F.; Nicoud, J.-F.; Nierengarten, J.-F.; Liu, S.-G.; Echegoyen, L.; Barigelletti, F.; Armaroli, N.; Ouali, L.; Krasnikov, V.; Hadziioannou, G. Fullerene−Oligophenylenevinylene Hybrids: Synthesis, Electronic Properties, and Incorporation in Photovoltaic Devices. *J. Am. Chem. Soc.* **2000**, *122*, 7467−7479.
(39) Meier, H.; Holst, H. C.; Oehlhof, A. Star-Shaped Compounds Having 1,3,5-Triazine Cores. *Eur. J. Org. Chem.* **2003**, *2003*, 4173−4180.
(40) Dierking, I. *Textures of Liquid Crystals*; Wiley-VCH: Weinheim, 2003.
(41) Pathak, S. K.; Nath, S.; De, J.; Pal, S. K.; Achalkumar, A. S. The Effect of Regioisomerism on the Mesomorphic and Photophysical Behavior of Oxadiazole-Based Tris(*N*-salicylideneaniline)s: Synthesis and Characterization. *New J. Chem.* **2017**, *41*, 9908−9917.
(42) Meier, H.; Lehmann, M.; Kolb, U. Stilbenoid Dendrimers. *Chem. − Eur. J.* **2000**, *6*, 2462−2469.
(43) Lehmann, M.; Köhn, C.; Meier, H.; Renker, S.; Oehlhof, A. Supramolecular Order of Stilbenoid Dendrons: Importance of Weak Interactions. *J. Mater. Chem.* **2006**, *16*, 441−451.
(44) Veerabhadraswamy, B. N.; Dambal, H. K.; Rao, D. S. S.; Yelamaggad, C. V. *s*-Triazine-Based Functional Discotic Liquid Crystals: Synthesis, Mesomorphism and Photoluminescence. *ChemPhysChem* **2016**, *17*, 2225−2237.
(45) Achalkumar, A. S.; Veerabhadraswamy, B. N.; Hiremath, U. S.; Rao, D. S. S.; Prasad, S. K.; Yelamaggad, C. V. Photoluminescent Discotic Liquid Crystals Derived From Tris(*N*-salicylideneaniline) and Stilbene Conjugates: Structure-Property Correlations. *Dyes Pigm.* **2016**, *132*, 291−305.
(46) Pathak, S. K.; Gupta, R. K.; Nath, S.; Rao, D. S. S.; Prasad, S. K.; Achalkumar, A. S. Columnar Self-Assembly of Star-Shaped Luminescent Oxadiazole and Thiadiazole Derivatives. *J. Mater. Chem. C* **2015**, *3*, 2940−2952.
(47) Pathak, S. K.; Pradhan, B.; Gupta, R. K.; Gupta, M.; Pal, S. K.; Achalkumar, A. S. Aromatic $\pi-\pi$ Driven Supergelation, Aggregation Induced Emission and Columnar Self-Assembly of Star-Shaped 1,2,4-Oxadiazole Derivatives. *J. Mater. Chem. C* **2016**, *4*, 6546−6561.
(48) Pathak, S. K.; Pradhan, B.; Gupta, M.; Pal, S. K.; Sudhakar, A. A. Liquid Crystalline Star-Shaped Supergelator Exhibiting Aggregation Induced Blue Light Emission. *Langmuir* **2016**, *32*, 9301−9312.
(49) Palmans, A. R.; Vekemans, J. A.; Fischer, H.; Hikmet, R. A.; Meijer, E. W. Extended-Core Discotic Liquid Crystals Based on the Intramolecular H-Bonding in *N*-Acylated 2,2′-Bipyridine-3,3′-Diamine Moieties. *Chem. − Eur. J.* **1997**, *3*, 300−307.
(50) Olate, F. A.; Parra, M. L.; Vergara, J. M.; Barberá, J.; Dahrouch, M. Star-Shaped Molecules as Functional Materials Based on 1,3,5-Benzenetriesters with Pendant 1,3,4-Thiadiazole Groups: Liquid Crystals, Optical, Solvatofluorochromic and Electrochemical Properties. *Liq. Cryst.* **2017**, *44*, 1173−1184.
(51) Valera, J. S.; Sánchez-Naya, R.; Ramírez, F. J.; Zafra, J. L.; Gomez, R.; Casado, J.; Sánchez, L. Solvent-Directed Helical Stereomutation Discloses Pathway Complexity on *N*-Heterotriangulene-Based Organogelators. *Chem. − Eur. J.* **2017**, *23*, 11141−11146.
(52) Chen, Z.; Lohr, A.; Saha-Möller, C. R.; Würthner, F. Self-Assembled π-Stacks of Functional Dyes in Solution: Structural and Thermodynamic Features. *Chem. Soc. Rev.* **2009**, *38*, 564−584.
(53) Smulders, M. M. J.; Nieuwenhuizen, M. M. L.; de Greef, T. F. A.; van der Schoot, P.; Schenning, A. P. H. J.; Meijer, E. W. How to Distinguish Isodesmic From Cooperative Supramolecular Polymerisation. *Chem. − Eur. J.* **2010**, *16*, 362−367.
(54) Mayoral, M. J.; Rest, C.; Schellheimer, J.; Stepanenko, V.; Fernández, G. Narcissistic versus Social Self-Sorting of Oligophenyleneethynylene Derivatives: From Isodesmic Self-Assembly to Cooperative Co-Assembly. *Chem. − Eur. J.* **2012**, *18*, 15607−15611.
(55) Ogi, S.; Stepanenko, V.; Sugiyasu, K.; Takeuchi, M.; Würthner, F. Mechanism of Self-Assembly Process and Seeded Supramolecular Polymerization of Perylene Bisimide Organogelator. *J. Am. Chem. Soc.* **2015**, *137*, 3300−3307.
(56) Kulkarni, C.; Bejagam, K. K.; Senanayak, S. P.; Narayan, K. S.; Balasubramanian, S.; George, S. J. Dipole-Moment-Driven Cooperative Supramolecular Polymerization. *J. Am. Chem. Soc.* **2015**, *137*, 3924−3932.
(57) Hifsudheen, M.; Mishra, R. K.; Vedhanarayanan, B.; Praveen, V. K.; Ajayaghosh, A. The Helix to Super-Helix Transition in the Self-Assembly of π-Systems: Superseding of Molecular Chirality at Hierarchical Level. *Angew. Chem., Int. Ed.* **2017**, *56*, 12634−12638.
(58) Greciano, E. E.; Sánchez, L. Seeded Supramolecular Polymerization in a Three-Domain Self-Assembly of an *N*-Annulated Perylenetetracarboxamide. *Chem. − Eur. J.* **2016**, *22*, 13724−13730.
(59) Greciano, E. E.; Matarranz, B.; Sánchez, L. Pathway Complexity Versus Hierarchical Self-Assembly in *N*-Annulated Perylenes: Structural Effects in Seeded Supramolecular Polymerization. *Angew. Chem., Int. Ed.* **2018**, *57*, 4697.
(60) Hollamby, M. J.; Karny, M.; Bomans, P. H. H.; Sommerdjik, N. A. J. M.; Saeki, A.; Seki, S.; Minamikawa, H.; Grillo, I.; Pauw, B. R.; Brown, P.; Eastoe, J.; Möhwald, H.; Nakanishi, T. Directed Assembly of Optoelectronically Active Alkyl−π-Conjugated Molecules by Adding *n*-Alkanes or π-Conjugated Species. *Nat. Chem.* **2014**, *6*, 690−696.
(61) Dasgupta, D.; Srinivasan, S.; Rochas, C.; Ajayaghosh, A.; Guenet, J.-M. Solvent-Mediated Fiber Growth in Organogels. *Soft Matter* **2011**, *7*, 9311−9315.
(62) Dasgupta, D.; Thierry, A.; Rochas, C.; Ajayaghosh, A.; Guenet, J. M. Key Role of Solvent Type in Organogelation. *Soft Matter* **2012**, *8*, 8714−8721.
(63) Lan, Y.; Corradini, M. G.; Weiss, R. G.; Raghavan, S. R.; Rogers, M. A. To Gel or Not to Gel-Correlating Molecular Gelation with Solvent Parameters. *Chem. Soc. Rev.* **2015**, *44*, 6035−6058.
(64) Chen, J. Y.; Yuan, B.; Li, Z. Y.; Tang, B.; Ankers, E.; Wang, X. G.; Li, J. L. Controlling the Supramolecular Architecture of Molecular Gels with Surfactants. *Langmuir* **2016**, *32*, 1171−1177.
(65) Prabhu, D. D.; Sivadas, A. P.; Das, S. Solvent Assisted Fluorescence Modulation of a C_3-Symmetric Organogelator. *J. Mater. Chem. C* **2014**, *2*, 7039−7046.
(66) Kim, T.; Mori, T.; Aida, T.; Miyajima, D. Dynamic Propeller Conformation for the Unprecedentedly High Degree of Chiral Amplification of Supramolecular Helices. *Chem. Sci.* **2016**, *7*, 6689−6694.
(67) van der Weegen, R.; Teunissen, A. J. P.; Meijer, E. W. Directing the Self-Assembly Behaviour of Porphyrin-Based Supramolecular Systems. *Chem. − Eur. J.* **2017**, *23*, 3773−3783.
(68) Kulkarni, C.; Korevaar, P. A.; Bejagam, K. K.; Palmans, A. R. A.; Meijer, E. W.; George, S. J. Solvent Clathrate Driven Dynamic Stereomutation of a Supramolecular Polymer with Molecular Pockets. *J. Am. Chem. Soc.* **2017**, *139*, 13867−13875.

DOI: 10.1021/acsomega.8b00496
ACS Omega 2018, 3, 4392−4399